PHYSICAL REVIEW B **92**, 155409 (2015)

Local spectroscopy of moiré-induced electronic structure in gate-tunable twisted bilayer graphene

Dillon Wong (黃家和),[1,2] Yang Wang (汪洋),[1,2] Jeil Jung (정재일),[3,4,5] Sergio Pezzini,[1,8] Ashley M. DaSilva,[4]
Hsin-Zon Tsai,[1,2] Han Sae Jung,[1,2,10] Ramin Khajeh,[1] Youngkyou Kim (김영규),[1,11] Juwon Lee (이주원),[1,2]
Salman Kahn (成吉思汗),[1,2] Sajjad Tollabimazraehno,[1,9] Haider Rasool,[1] Kenji Watanabe,[7] Takashi Taniguchi,[7] Alex Zettl,[1,2]
Shaffique Adam,[5,6] Allan H. MacDonald,[4] and Michael F. Crommie[1,2,*]
[1]*Department of Physics, University of California at Berkeley, Berkeley, California 94720, USA*
[2]*Materials Science Division, Lawrence Berkeley National Laboratory, Berkeley, California 94720, USA*
[3]*Department of Physics, University of Seoul, Seoul 130-743, Korea*
[4]*Department of Physics, University of Texas at Austin, Austin, Texas 78712, USA*
[5]*Physics Department, National University of Singapore, 117551, Singapore*
[6]*Yale-NUS College, 138614, Singapore*
[7]*National Institute for Materials Science, Tsukuba, Ibaraki 305-0044, Japan*
[8]*Dipartimento di Fisica, Università degli studi di Pavia, I-27100 Pavia, Italy*
[9]*Johannes Kepler University Linz, 4040 Linz, Austria*
[10]*Department of Chemistry, University of California at Berkeley, Berkeley, California 94720, USA*
[11]*Department of Chemical and Biomolecular Engineering, University of California at Berkeley, Berkeley, California 94720, USA*
(Received 10 August 2015; published 7 October 2015)

Twisted bilayer graphene (tBLG) forms a quasicrystal whose structural and electronic properties depend on the angle of rotation between its layers. Here, we present a scanning tunneling microscopy study of gate-tunable tBLG devices supported by atomically smooth and chemically inert hexagonal boron nitride (BN). The high quality of these tBLG devices allows identification of coexisting moiré patterns and moiré super-superlattices produced by graphene-graphene and graphene-BN interlayer interactions. Furthermore, we examine additional tBLG spectroscopic features in the local density of states beyond the first van Hove singularity. Our experimental data are explained by a theory of moiré bands that incorporates *ab initio* calculations and confirms the strongly nonperturbative character of tBLG interlayer coupling in the small twist-angle regime.

DOI: 10.1103/PhysRevB.92.155409 PACS number(s): 73.20.At, 73.22.Pr

Van der Waals heterostructures [1] built from rotated layered materials exhibit novel electronic structure, including van Hove singularities (VHSs) [2], massive Dirac fermions [3], superlattice Dirac points [4], and the Hofstadter butterfly [5,6]. Twisted bilayer graphene (tBLG) is a model system for studying such heterostructures, because it is composed of two identical stacked sheets of graphene oriented with a relative twist angle between them. Interactions between the two graphene layers result in a moiré pattern with a superlattice period that scales inversely with the twist angle [7–10] and produce dramatic modifications to the graphene electronic properties [11–20]. For example, overlap between the two layers' Dirac cones leads to an avoided crossing and a resulting VHS peak in the density of states (DOS) [2,9,21]. Although the formation of the VHS has previously been reported for tBLG samples, the substrates used in those papers (silicon carbide, graphite, and metals) influence the tBLG electronic structure and thus complicate its interpretation [2,9,22,23]. This has led to discrepancies among measurements performed on different tBLG samples [2,9,23]. Electronic structure measurements of tBLG on less interacting substrates, such as hexagonal boron nitride (BN) [24–27], are therefore necessary to understand the intrinsic properties of tBLG.

Here, we report on a scanning tunneling microscopy (STM) study of electrostatically gated tBLG supported by a BN substrate (tBLG/BN). The high quality of our tBLG/BN devices enables us to visualize new tBLG phenomena on multiple length scales, from atomic lattices to moiré super-superlattices. Although coexisting moiré patterns have previously been observed in graphitic multilayers [9,10], we demonstrate here that moiré patterns produced by graphene-graphene interlayer interactions can coincide with moiré patterns that arise from graphene-BN interactions to produce a new super-superlattice structure. Our scanning tunneling spectroscopy (STS) measurements of tBLG/BN yield new insight into how the intrinsic electronic behavior of tBLG is affected by moiré-induced interactions. For example, we observe an additional dip feature in the DOS at an energy beyond the first VHS. By comparing the moiré wavelength dependence of this new feature's energy to calculations incorporating *ab initio* results, we find that it arises from a partial gap opening between the second and the third moiré bands due to strong nonperturbative interlayer coupling in the small twist-angle regime. These measurements on our high-quality tBLG/BN samples provide a first look into the atomic-scale behavior of electrostatically gated tBLG, an important device configuration for future applications [28,29].

Our measurements were performed using an Omicron ultra-high-vacuum (UHV) STM operating at temperature $T = 5\,\mathrm{K}$ with electrochemically etched PtIr tips. The tips were calibrated against the surface state of an Au(111) crystal before performing all measurements [30]. Differential conductance (dI/dV) was measured by lock-in detection of the tunneling current modulated by a 6 to 8 meV (root mean square), 400 to 700 Hz signal added to the sample bias (V_s). Each tBLG device was fabricated by growing two monolayers of graphene via chemical vapor deposition (CVD) [31] and then sequentially transferring the layers onto a BN flake peeled onto an SiO_2/Si

---

[*] Corresponding author: crommie@berkeley.edu

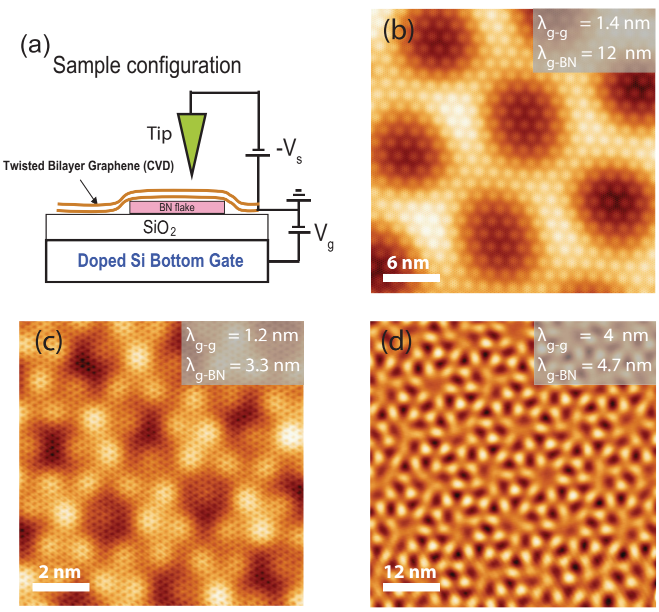

FIG. 1. (Color online) STM topographic images of tBLG/BN. (a) Gated tBLG/BN field effect transistor. The tip bias ($-V_s$), back-gate voltage (V_g), and grounding scheme are shown. (b)–(d) STM topographic images show coexisting graphene-graphene and graphene-BN moiré patterns. Tunneling parameters: (b) $V_s = -0.2\,\mathrm{V}$, $I = 0.30\,\mathrm{nA}$, $V_g = 0\,\mathrm{V}$; (c) $V_s = -0.3\,\mathrm{V}$, $I = 0.30\,\mathrm{nA}$, $V_g = +30\,\mathrm{V}$; (d) $V_s = -3.0\,\mathrm{V}$, $I = 0.02\,\mathrm{nA}$, $V_g = 0\,\mathrm{V}$.

wafer [see Fig. 1(a) for a schematic of a typical graphene device; see Ref. [32] for more details about the growth and transfer processes]. The samples were annealed in UHV at 400 °C for several hours to clean them before loading them into the STM.

The CVD-grown graphene used here was multicrystalline with grain sizes on the order of several microns, so the stacking of the two graphene layers naturally resulted in a multitude of random twist angles θ_{g-g} (angle between the two graphene layers) and θ_{g-BN} (angle between the bottom graphene layer and the BN) across the entire sample. This is confirmed by the STM topographic images of Fig. 1(b)–1(d), which display different areas exhibiting different moiré wavelengths from different spots on the same sample. Figure 1(b) and 1(c) shows graphene-graphene moiré patterns coexisting with graphene-BN moiré patterns, with the atomic lattice of the top graphene layer also visible (the atomic-scale structure can be more clearly seen in a higher magnification image in Supplemental Material [33]). The presence of these moiré patterns indicates that the interfaces between the graphene and the BN layers are atomically sharp and free from contamination. The origins of the different moiré patterns are easily distinguished since the depressions in the graphene-graphene moiré pattern form a honeycomblike appearance, whereas the depressions in the graphene-BN moiré pattern resemble a triangular lattice. Figure 1(b) exhibits a graphene-graphene moiré wavelength $\lambda_{g-g} = 1.4\,\mathrm{nm}$ and a graphene-BN moiré wavelength $\lambda_{g-BN} = 12\,\mathrm{nm}$, while Fig. 1(c) has $\lambda_{g-g} = 1.2\,\mathrm{nm}$ and $\lambda_{g-BN} = 3.3\,\mathrm{nm}$.

In contrast to Fig. 1(b) and 1(c), where λ_{g-BN} is much larger than λ_{g-g}, Fig. 1(d) depicts a pair of coexisting moiré patterns where $\lambda_{g-BN} \approx \lambda_{g-g}$. When two moiré patterns are of similar size, they interfere to produce a moiré of the moirés. This new super-superlattice structure can be shown to have a wavelength given by

$$\lambda_S = \frac{\lambda_{g-BN}}{\sqrt{\left(\frac{\lambda_{g-BN}}{\lambda_{g-g}}\right)^2 + 1 - 2\left(\frac{\lambda_{g-BN}}{\lambda_{g-g}}\right)\cos(\Delta\theta)}}$$

where $\Delta\theta$ is the rotation angle between the graphene-graphene moiré and the graphene-BN moiré. We are able to extract $\lambda_{g-BN} = 4.7\,\mathrm{nm}$, $\lambda_{g-g} = 4\,\mathrm{nm}$, and $\Delta\theta = 18^\circ$ through a Fourier transform of Fig. 1(d) (see Supplemental Material [33]). These values yield $\lambda_S = 12\,\mathrm{nm}$, consistent with direct measurement of the super-superlattice periodicity in Fig. 1(d).

In order to explore the intrinsic behavior of tBLG, we performed STM measurements on regions of our device with $\theta_{g-BN} > 15^\circ$. Atomically resolved topographic images of such regions are depicted in Fig. 2 and do not show any features arising from the underlying BN substrate. The twist angle θ_{g-g} for each region is obtained through the observed moiré period λ_{g-g} with the relation [7,12]

$$\lambda_{g-g} = \frac{a}{2\sin\frac{\theta_{g-g}}{2}}$$

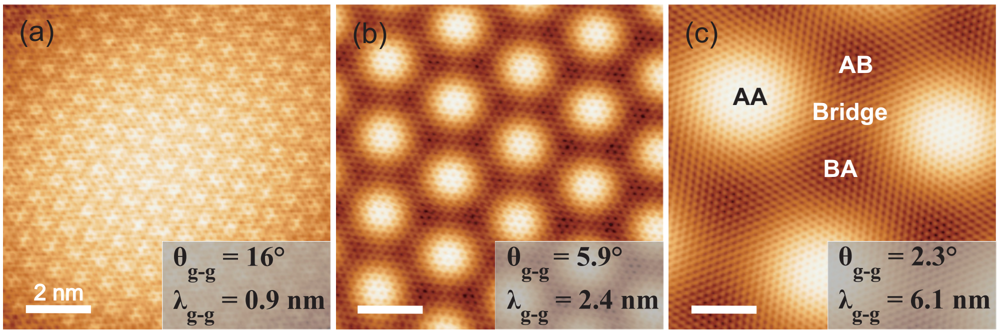

FIG. 2. (Color online) STM topographic images of tBLG/BN for different graphene-graphene twist angles. (a)–(c) STM topographic images of tBLG show both the top-layer atomic lattices and the graphene-graphene moiré patterns for decreasing twist angle θ_{g-g}. No graphene-BN moiré patterns are visible in these images since $\theta_{g-BN} > 15^\circ$. Tunneling parameters: (a) $V_s = -0.5\,\mathrm{V}$, $I = 0.1\,\mathrm{nA}$, $V_g = 0\,\mathrm{V}$; (b) $V_s = -0.5\,\mathrm{V}$, $I = 0.2\,\mathrm{nA}$, $V_g = +30\,\mathrm{V}$; (c) $V_s = -0.1\,\mathrm{V}$, $I = 0.1\,\mathrm{nA}$, $V_g = -60\,\mathrm{V}$.

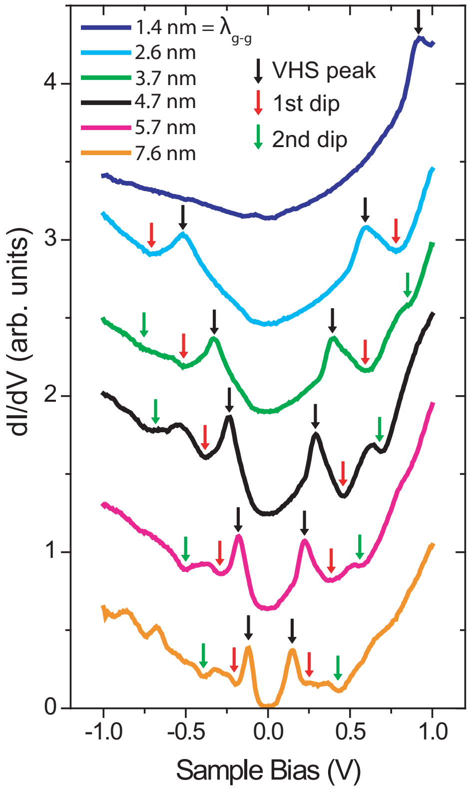

FIG. 3. (Color online) STM dI/dV spectra of tBLG for different graphene-graphene moiré wavelengths. The dI/dV spectra reveal three features (the VHS peak labeled by a black arrow, first dip labeled by a red arrow, and second dip labeled by a green arrow) that disperse with graphene-graphene moiré wavelength λ_{g-g}. Curves have been shifted vertically for clarity. Initial tunneling parameters: $V_s = 1$ V, 0.2 nA $\leqslant I \leqslant$ 0.4 nA, ac modulation 6 mV $\leqslant V_{\mathrm{rms}} \leqslant$ 8 mV.

where $a = 2.46$ Å is the graphene lattice constant. We verify that the moiré patterns are created by the graphene-graphene interaction and not the graphene-BN interaction by comparing the relative orientations of the top-layer graphene lattice and the moiré lattice. Figure 2(a)–2(c) display graphene-graphene moiré wavelengths 0.9, 2.4, and 6.1 nm, corresponding to θ_{g-g} twist angles 16°, 5.9°, and 2.3°, respectively. As the twist angle decreases, the local AA stacked regions (where top and bottom graphene sublattices are aligned) and AB stacked regions (where Bernal stacking occurs) become better defined [Fig. 2(c)]. Each AA region displays an internal honeycomblike structure, while the AB/BA regions display internal triangularlike lattice structures with opposite orientations (consistent with the expected tBLG structure [13,34–37]).

The local electronic structure of tBLG/BN in the $\theta_{g-BN} > 15°$ regime was measured by performing STM dI/dV spectroscopy in areas that have different moiré wavelengths λ_{g-g} (see Supplemental Material [33] for spectroscopy in areas with $\theta_{g-BN} < 15°$). Figure 3 shows dI/dV spectra obtained in the AA regions of different moiré patterns (spectra obtained in AB/BA and bridge moiré regions are quite similar; see Supplemental Material [33]). All spectra in Fig. 3 were taken while holding the Dirac point close to (but not exactly at) the Fermi level via application of a gate voltage (V_g). The Dirac point feature is not clearly visible in these spectra because of a ~130-meV-wide gaplike feature at the Fermi level that is caused by phonon-assisted inelastic tunneling (similar to the case for monolayer graphene [38]). Our spectra exhibit a peak and two dips (labeled by colored arrows) that disperse with the moiré wavelength. The peak (black arrows) corresponds to the VHS previously reported by STS and angle-resolved photoemission spectroscopy [2,9,22], the first dip (red arrows) is a minima that follows the VHS, and the second dip (green arrows) is a phenomenon not present in previous papers on tBLG on graphite or silicon carbide substrates [2,9]. The energy magnitudes of these features (relative to the Dirac point) decrease as the moiré wavelength increases, and each feature has a symmetric copy lying on the opposite side of the Dirac point.

Figure 4(a) shows a plot of the energy magnitudes of the three observed features (relative to the Dirac point) versus the moiré wavelength λ_{g-g} (error bars are approximately the size of the symbols). The gate tunability of our tBLG devices was crucial to maintain accuracy for this measurement since the measurement had to be performed under a condition of high carrier density (mid 10^{12} cm^{-2}) by setting the back-gate voltage V_g to +60 or −60 V. This allowed the Fermi level (E_{F}) to be positioned such that DOS(E_{F}) is as high as possible, thus reducing the effect of tip-induced band bending compared to the case where E_{F} is positioned near the Dirac point [39] (which has low DOS) (see Supplemental Material [33] for a comparison between spectroscopic features measured at different carrier doping levels).

We carried out theoretical simulations and compared them to our experimental data in order to interpret the observed spectroscopic features. While the tBLG VHS is typically thought of as a saddle point generated by avoided crossing between rotated Dirac cones [2,9,40–42], it can more generally be thought of as the result of a collection of zone-folded Bloch bands arising from the periodicity associated with the moiré pattern [43]. In this picture, the avoided crossing that gives rise to the VHS (i.e., the first dip) is the energy gap between the first and the second moiré Bloch bands, and higher order gaps are expected. We modeled this behavior through an effective Hamiltonian formalism that allowed us to calculate the tBLG electronic band structure, total DOS, and local density of states (LDOS) for arbitrary bilayer twist angles [44] (see Supplemental Material for LDOS simulations [33]). This technique incorporates *ab initio* calculations performed in commensurate periodic structures as input to construct the effective Hamiltonian and allows vertical relaxation of the interlayer separation (see Ref. [44] for details). This theory has no adjustable parameters other than the value of the unperturbed graphene Fermi velocity $v_F = 1.05 \times 10^6$ m/s (Supplemental Material [33] shows calculations for different values of v_F). A schematic plot of the momentum space structure of tBLG in a repeated zone scheme is shown in Fig. 4(b). The green line here represents the Wigner-Seitz cell of the moiré reciprocal lattice, while the red and black circles mark the Dirac points of the two graphene layers. Special high-symmetry points in the Brillouin zone are labeled A–D. The resulting moiré-induced band structure of tBLG for $\lambda_{g-g} = 7.6$ nm is plotted in Fig. 4(c) (band structure plots for different λ_{g-g} are shown in Supplemental Material [33]). The corresponding integrated DOS is displayed in Fig. 4(d) and

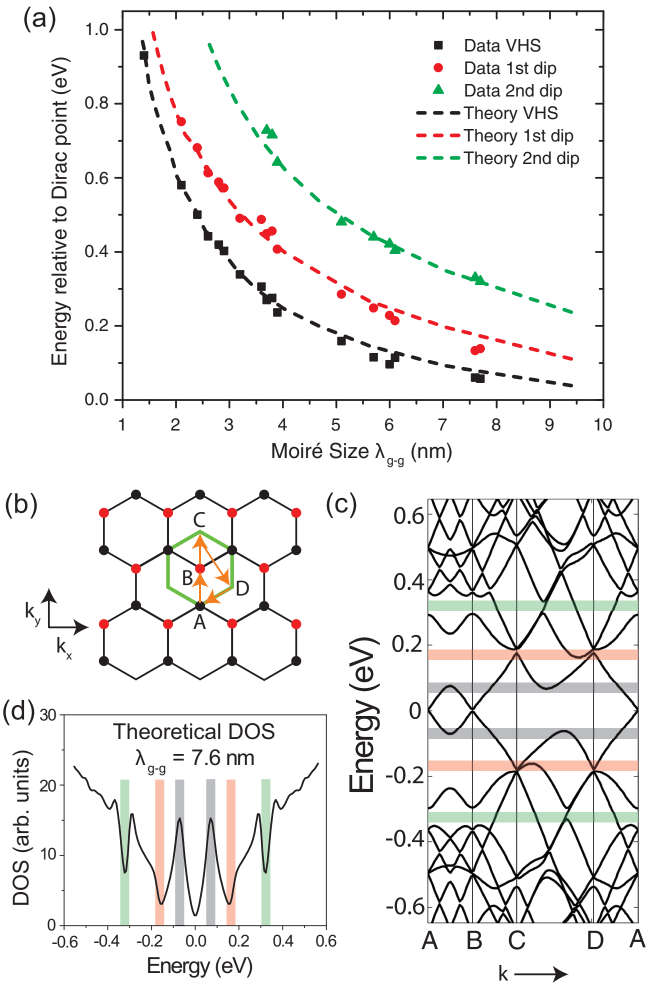

FIG. 4. (Color online) Calculated tBLG electronic structure. (a) Dependence of theoretical tBLG spectroscopic features on moiré wavelength λ_{g-g} (dashed lines) compared to experiment (symbols). Experimental error bars are approximately the size of the symbols. (b) Schematic plot of the repeated-zone momentum space structure of tBLG. The Wigner-Seitz cell (green line) of the moiré reciprocal lattice and the Dirac points of the two graphene layers (red and black circles) are shown. A–D mark high symmetry points in the moiré Brillouin zone. (c) Calculated moiré-induced band structure of tBLG for $\lambda_{g-g} = 7.6$ nm plotted along k space lines connecting points A-B-C-D-A in (b). Gray, red, and green highlights locate the energies of the VHS peak, the first dip, and the second dip, respectively. (d) Theoretical DOS of tBLG for $\lambda_{g-g} = 7.6$ nm calculated by integrating the band structure over the moiré Brillouin zone and then Gaussian broadening with a 15 meV width (the broadening represents the effects of temperature, finite quasiparticle lifetime, and ac wiggle voltage). The semitransparent highlighting bars are located at the same energies as in (c) and match the three spectroscopic features observed in the experiment.

shows features that match our experimental results reasonably well (e.g., a peak and two dips, highlighted in semitransparent color bars). A good match between theory and experiment is also seen for the energy magnitudes of the calculated spectroscopic features as a function of moiré wavelength [Fig. 4(a)], as well as for our energy-dependent dI/dV maps (see Supplemental Material [33]).

The quantitative agreement between our theoretical calculations and experimental data enables us to identify the physical origin of the experimentally observed features. For example, the first dip seen in the dI/dV spectroscopy can be identified as a partial gap opening between the first and the second moiré bands [red highlighted bars in Fig. 4(c) and 4(d)], while the new second dip feature is seen to correspond to the gap between the second and the third moiré bands [green highlighted bars in Fig. 4(c) and 4(d)]. Our paper thus demonstrates the validity of the moiré bands picture of tBLG even for incommensurate orientations of the two graphene layers.

The moiré wavelength dependence of the spectroscopic features observed here also reveals the nonperturbative nature of the graphene interlayer interaction. As seen in Fig. 4(a), the energy of the VHS scales inversely with moiré wavelength for both theory and experiment. However, this is not the case for the first dip, where $1/\lambda_{g-g}$ scaling is not preserved for larger moiré periods (see Supplemental Material [33]). Inverse scaling with the moiré period, a signature of the perturbative regime, only occurs for large twist angles (small moiré wavelengths). For small twist angles (long moiré wavelengths), we find deviations from inverse scaling for the first dip, a signature of the nonperturbative interaction between the two graphene layers in this regime.

Due to this nonperturbative interaction, tBLG is quite different from the case of monolayer graphene supported by BN. The interaction between monolayer graphene and BN induces a simple periodic perturbation, which gives rise to superlattice-induced mini-Dirac points in graphene [4,45–47]. Accurate parameterization of the moiré pattern site energy, local gap, and pseudogauge virtual strain terms has been presented for graphene on BN. However, the coupling between two graphene layers in tBLG cannot be reduced to effective periodic potentials within each independent layer [44]. The strong interlayer coupling in tBLG can be seen by examining the band structure plot of Fig. 4(c) more carefully. Two Dirac-cone-like features are seen at points C and D near the energy window of the first dip (red bar), but no mini-Dirac cones are seen in the energy window of the second dip (green bar). Overall, the moiré band features of tBLG are in stark contrast to the case of monolayer graphene on BN [47].

In conclusion, we have fabricated gate-tunable tBLG devices using high quality BN substrates and demonstrated that graphene-graphene moiré patterns can exist simultaneously with graphene-BN moiré patterns. The existence of these coexisting moiré patterns may have important consequences for device applications involving stacked graphene and BN layers, and the emergence of graphene-BN super-superlattices may serve as an interesting platform for novel physical phenomena. The high quality of our tBLG/BN devices has enabled us to probe the intrinsic electronic properties of tBLG and to observe new spectroscopic features in the tBLG DOS. These features occur at energies beyond the first VHS and can be explained by a nonperturbative theory involving *ab initio* calculations. These results show that the strong coupling, low twist-angle regime in tBLG can be accessed using scanned probe techniques via high quality devices that allow electrostatic Fermi level tuning.

We thank Feng Wang for useful discussions. This research was supported by the Department of Energy under Contracts No. DE-AC02-05CH11231 (sp^2 program) (STM imaging and spectroscopy) and No. DE-FG02-ER45118 (development of effective Hamiltonian formalism), the National Science Foundation under Grant No. DMR-1206512 (sample fabrication), the National Research Foundation of Singapore under its fellowship program through Grant No. NRF-NRFF2012-01 (tBLG DOS and LDOS simulations), and the Elemental Strategy Initiative conducted by the Ministry of Education, Culture, Sports, Science and Technology, Japan (BN synthesis). D.W. was supported by the Department of Defense through the National Defense Science & Engineering Graduate Fellowship Program, Grant No. 32 CFR 168a. T.T. acknowledges support from a Grant-in-Aid for Scientific Research No. 262480621 (BN crystal characterization) and a Grant-in-Aid for Innovative Areas "NanoInformatics" No. 25106006 (development of BN synthesis instrumentation) from the Japan Society for the Promotion of Science.

D.W., Y.W., and J.J. contributed equally to this paper.

---

[1] A. K. Geim and I. V. Grigorieva, Nature **499**, 419 (2013).

[2] G. Li, A. Luican, J. M. B. Lopes dos Santos, A. H. Castro Neto, A. Reina, J. Kong, and E. Y. Andrei, Nat. Phys. **6**, 109 (2010).

[3] B. Hunt, J. D. Sanchez-Yamagishi, A. F. Young, M. Yankowitz, B. J. LeRoy, K. Watanabe, T. Taniguchi, P. Moon, M. Koshino, P. Jarillo-Herrero, and R. C. Ashoori, Science **340**, 1427 (2013).

[4] M. Yankowitz, J. Xue, D. Cormode, J. D. Sanchez-Yamagishi, K. Watanabe, T. Taniguchi, P. Jarillo-Herrero, P. Jacquod, and B. J. LeRoy, Nat. Phys. **8**, 382 (2012).

[5] C. R. Dean, L. Wang, P. Maher, C. Forsythe, F. Ghahari, Y. Gao, J. Katoch, M. Ishigami, P. Moon, M. Koshino, T. Taniguchi, K. Watanabe, K. L. Shepard, J. Hone, and P. Kim, Nature **497**, 598 (2013).

[6] L. A. Ponomarenko, R. V. Gorbachev, G. L. Yu, D. C. Elias, R. Jalil, A. A. Patel, A. Mishchenko, A. S. Mayorov, C. R. Woods, J. R. Wallbank, M. Mucha-Kruczynski, B. A. Piot, M. Potemski, I. V. Grigorieva, K. S. Novoselov, F. Guinea, V. I. Fal'ko, and A. K. Geim, Nature **497**, 594 (2013).

[7] S. Shallcross, S. Sharma, E. Kandelaki, and O. A. Pankratov, Phys. Rev. B **81**, 165105 (2010).

[8] C.-C. Lu, Y.-C. Lin, Z. Liu, C.-H. Yeh, K. Suenaga, and P.-W. Chiu, ACS Nano **7**, 2587 (2013).

[9] I. Brihuega, P. Mallet, H. González-Herrero, G. Trambly de Laissardière, M. M. Ugeda, L. Magaud, J. M. Gómez-Rodríguez, F. Ynduráin, and J. Y. Veuillen, Phys. Rev. Lett. **109**, 196802 (2012).

[10] D. L. Miller, K. D. Kubista, G. M. Rutter, M. Ruan, W. A. de Heer, P. N. First, and J. A. Stroscio, Phys. Rev. B **81**, 125427 (2010).

[11] J. M. B. Lopes dos Santos, N. M. R. Peres, and A. H. Castro Neto, Phys. Rev. Lett. **99**, 256802 (2007).

[12] J. M. B. Lopes dos Santos, N. M. R. Peres, and A. H. Castro Neto, Phys. Rev. B **86**, 155449 (2012).

[13] P. San-Jose, J. González, and F. Guinea, Phys. Rev. Lett. **108**, 216802 (2012).

[14] Z.-D. Chu, W.-Y. He, and L. He, Phys. Rev. B **87**, 155419 (2013).

[15] E. J. Mele, Phys. Rev. B **84**, 235439 (2011).

[16] E. Suárez Morell, J. D. Correa, P. Vargas, M. Pacheco, and Z. Barticevic, Phys. Rev. B **82**, 121407 (2010).

[17] G. Trambly de Laissardière, D. Mayou, and L. Magaud, Phys. Rev. B **86**, 125413 (2012).

[18] M. Sprinkle, D. Siegel, Y. Hu, J. Hicks, A. Tejeda, A. Taleb-Ibrahimi, P. Le Fèvre, F. Bertran, S. Vizzini, H. Enriquez, S. Chiang, P. Soukiassian, C. Berger, W. A. de Heer, A. Lanzara, and E. H. Conrad, Phys. Rev. Lett. **103**, 226803 (2009).

[19] D. A. Siegel, C. G. Hwang, A. V. Fedorov, and A. Lanzara, Phys. Rev. B **81**, 241417 (2010).

[20] P. Moon and M. Koshino, Phys. Rev. B **87**, 205404 (2013).

[21] A. Luican, G. Li, A. Reina, J. Kong, R. R. Nair, K. S. Novoselov, A. K. Geim, and E. Y. Andrei, Phys. Rev. Lett. **106**, 126802 (2011).

[22] T. Ohta, J. T. Robinson, P. J. Feibelman, A. Bostwick, E. Rotenberg, and T. E. Beechem, Phys. Rev. Lett. **109**, 186807 (2012).

[23] W. Yan, M. Liu, R.-F. Dou, L. Meng, L. Feng, Z.-D. Chu, Y. Zhang, Z. Liu, J.-C. Nie, and L. He, Phys. Rev. Lett. **109**, 126801 (2012).

[24] C. R. Dean, A. F. Young, I. Meric, C. Lee, L. Wang, S. Sorgenfrei, K. Watanabe, T. Taniguchi, P. Kim, K. L. Shepard, and J. Hone, Nat. Nano **5**, 722 (2010).

[25] J. Xue, J. Sanchez-Yamagishi, D. Bulmash, P. Jacquod, A. Deshpande, K. Watanabe, T. Taniguchi, P. Jarillo-Herrero, and B. J. LeRoy, Nat. Mater. **10**, 282 (2011).

[26] R. Decker, Y. Wang, V. W. Brar, W. Regan, H.-Z. Tsai, Q. Wu, W. Gannett, A. Zettl, and M. F. Crommie, Nano Lett. **11**, 2291 (2011).

[27] D. Wong, J. Velasco Jr, L. Ju, J. Lee, S. Kahn, H.-Z. Tsai, C. Germany, T. Taniguchi, K. Watanabe, A. Zettl, F. Wang, and M. F. Crommie, Nat. Nano (2015).

[28] Y. Kim, H. Yun, S.-G. Nam, M. Son, D. S. Lee, D. C. Kim, S. Seo, H. C. Choi, H.-J. Lee, S. W. Lee, and J. S. Kim, Phys. Rev. Lett. **110**, 096602 (2013).

[29] J. D. Sanchez-Yamagishi, T. Taychatanapat, K. Watanabe, T. Taniguchi, A. Yacoby, and P. Jarillo-Herrero, Phys. Rev. Lett. **108**, 076601 (2012).

[30] W. Chen, V. Madhavan, T. Jamneala, and M. F. Crommie, Phys. Rev. Lett. **80**, 1469 (1998).

[31] X. Li, W. Cai, J. An, S. Kim, J. Nah, D. Yang, R. Piner, A. Velamakanni, I. Jung, E. Tutuc, S. K. Banerjee, L. Colombo, and R. S. Ruoff, Science **324**, 1312 (2009).

[32] H. S. Jung, H.-Z. Tsai, D. Wong, C. Germany, S. Kahn, Y. Kim, A. S. Aikawa, D. K. Desai, G. F. Rodgers, A. J. Bradley, J. Velasco Jr., K. Watanabe, T. Taniguchi, F. Wang, A. Zettl, and M. F. Crommie, J. Vis. Exp. e52711 (2015).

[33] See Supplemental Material at http://link.aps.org/supplemental/10.1103/PhysRevB.92.155409 for additional data.

[34] G. Trambly de Laissardière, D. Mayou, and L. Magaud, Nano Lett. **10**, 804 (2010).

[35] W. Landgraf, S. Shallcross, K. Türschmann, D. Weckbecker, and O. Pankratov, Phys. Rev. B **87**, 075433 (2013).

[36] S. Latil, V. Meunier, and L. Henrard, Phys. Rev. B **76**, 201402 (2007).

[37] S. Shallcross, S. Sharma, and O. Pankratov, Phys. Rev. B **87**, 245403 (2013).

[38] Y. Zhang, V. W. Brar, F. Wang, C. Girit, Y. Yayon, M. Panlasigui, A. Zettl, and M. F. Crommie, Nat. Phys. **4**, 627 (2008).

[39] V. W. Brar, R. Decker, H.-M. Solowan, Y. Wang, L. Maserati, K. T. Chan, H. Lee, Ç. O. Girit, A. Zettl, S. G. Louie, M. L. Cohen, and M. F. Crommie, Nat. Phys. **7**, 43 (2011).

[40] R. W. Havener, H. Zhuang, L. Brown, R. G. Hennig, and J. Park, Nano Lett. **12**, 3162 (2012).

[41] K. Kim, S. Coh, L. Z. Tan, W. Regan, J. M. Yuk, E. Chatterjee, M. F. Crommie, M. L. Cohen, S. G. Louie, and A. Zettl, Phys. Rev. Lett. **108**, 246103 (2012).

[42] R. He, T.-F. Chung, C. Delaney, C. Keiser, L. A. Jauregui, P. M. Shand, C. C. Chancey, Y. Wang, J. Bao, and Y. P. Chen, Nano Lett. **13**, 3594 (2013).

[43] R. Bistritzer and A. H. MacDonald, Proc. Natl. Acad. Sci. USA **108**, 12233 (2011).

[44] J. Jung, A. Raoux, Z. Qiao, and A. H. MacDonald, Phys. Rev. B **89**, 205414 (2014).

[45] C.-H. Park, L. Yang, Y.-W. Son, M. L. Cohen, and S. G. Louie, Nat. Phys. **4**, 213 (2008).

[46] C. H. Park, L. Yang, Y. W. Son, M. L. Cohen, and S. G. Louie, Phys. Rev. Lett. **101**, 126804 (2008).

[47] J. Jung, A. M. DaSilva, A. H. MacDonald, and S. Adam, Nat. Comm. **6**, 6308 (2015).